Molecular Dynamics Study of the Effect of Surface Topography on Sputtering Induced by 20 keV Au_3 and C_{60} Clusters†

Robert Paruch,‡ Lukasz Rzeznik,‡ Michael F Russo,§ Barbara J. Garrison,§ and Zbigniew Postawa*,‡

Smoluchowski Institute of Physics, Jagiellonian University, Reymonta 4, 30-059 Kraków, Poland, and Department of Chemistry, The Pennsylvania State University, 104 Chemistry Bldg, University Park, Pennsylvania 16802

Received: June 30, 2009; Revised Manuscript Received: October 9, 2009

Molecular dynamics computer simulations are employed to investigate, at the atomic scale, the process of Ag(111) surface erosion stimulated by continuous bombardment by 20-keV Au_3 and C_{60} clusters at 0° and 70° impact angles. The surface modification, the total sputtering yield, and the kinetic energy and angular distributions of ejected species are calculated at fluences ranging from 0 up to $\sim 3 \times 10^{13}$ impacts/cm^2. It is shown that Au_3 irradiation leads to a more corrugated surface as compared to C_{60} bombardment. The development of the surface topography and aggregated alteration of the bulk have a significant influence on the total sputtering yield and the angular spectra, whereas the shape of the kinetic energy distributions are not sensitive to the modification of the sample morphology.

Introduction

Bombardment of solids by energetic clusters has drawn significant attention since it has been found experimentally that a nonlinear or nonadditive enhancement of the sputtering or ejection yield occurs relative to bombardment by atomic projectiles.[1,2] Since then numerous studies using both analytical approaches and computer modeling have been performed investigating processes stimulated by cluster impacts.[3−5] In general, it has been found that the presence of the nonlinear yield enhancement is associated with the formation of a region of a high density of deposited energy. In this region the assumption of binary collisions (linearity or one particle hitting another particle) is not fulfilled. This nonlinear behavior stimulated by energetic cluster bombardment has also found numerous practical applications. One of the most important applications is 3-dimensional chemical imaging by secondary ion mass spectrometry (SIMS).[6−10] In SIMS, the application of clusters such as SF_5, Au_3, Bi_3, and C_{60} which has been shown to stimulate a nonlinear enhancement of ion yield,[11,12] reduced chemical damage,[13] and reduced damage depth, has opened the door to a wide array of depth profiling capabilities, particularly of organic materials (see refs 14−16 for a review).

Currently the most popular cluster projectiles used in SIMS are Au_n/Bi_n ($n = 2$ or 3) and C_{60}. In the past several years, there have been numerous computational studies that investigated the dynamics of sputtering by these projectiles.[5,17−39] However, almost all of these studies were performed on a flat surface, in other words, the investigated impacts were independent and reflect the experimental condition of zero fluence. In fact, this approach is the one used over the years to model sputtering effects.[4,5] The results of computer simulations performed on flat surfaces are often related to experimental results, sometimes even those obtained at high fluence conditions. Surface topography does develop under high fluence conditions resulting in a surface that is far from flat;[40,41] therefore, it is relevant to verify to what extent such a comparison is justifiable. Performing simulations of high fluence experiments, however, is computationally challenging. Only a few attempts have been done to date to trace accumulated effects by multiple impacts of cluster projectiles or to probe processes stimulated by single impacts at artificially modified surfaces. Moseler at al. investigated the smoothing of thin film growth due to an energetic cluster impact on "tilted" areas of the film.[42] Aoki at al. utilized a Si sample covered with artificially placed geometrical blocks[43] or a sample with predefined, sine wave, surface features[44] to examine the effects that the surface roughness on a smoothing process by Ar clusters of hundreds to thousands of atoms.

The main goal of this paper is, therefore, to discuss similarities and differences that occur in development of surface topography induced by impact of 20 keV Au_3 and C_{60} cluster projectiles and to check if, and to what extent, the development of the surface topography can influence such characteristics as the total sputtering yield, the kinetic energy and angular distributions of sputtered particles. The ability to perform such simulations is made possible by a recently developed "divide and conquer" scheme for performing sequential impacts.[39]

Model. Details of MD computer simulations used to model cluster bombardment are described elsewhere.[5] Briefly, the motion of the particles is determined by integrating Hamilton's equations of motion. A "divide and conquer" scheme for performing several impacts simultaneously, while preserving the time dependence of the impact sequence has been developed.[39] Briefly, the procedure consists of the following steps: (1) Generate a large sample to be used for the depth profiling study. (2) Using random numbers, generate a list of impact coordinates. (3) Determine the size of a local sample that is needed to contain a single bombardment event. (4) Choose which impacts from the list of random points can be run at the same time. The critical consideration is that the random order should not be altered. The choice of simultaneous impacts is

† Part of the "Barbara J. Garrison Festschrift".

* Corresponding author. E-mail: zbigniew.postawa@if.uj.edu.pl.
‡ Jagiellonian University.
§ The Pennsylvania State University.

10.1021/jp906139d
Published on Web 12/02/2009

done by using a following criterion: the impact in question cannot have its local sample overlap any of the impacts already selected to be run concurrently. (5) Copy the coordinates of all the particles within a local sample to a separate file, using periodic boundary conditions around the main sample if necessary. (6) Run a group of noninteracting impacts simultaneously as individual simulations. (7) After the simulations have ended, replace the old coordinates with the new ones for each particle that was active. Such reinsertion is possible because samples used to calculate each impact do not overlap and the outer region of each sample (with exception of the surface) is composed from rigid atoms, which act as a sleeve (see below). (8) Repeat the same procedure for the next round of impacts, which will now take place on a modified surface.

The main sample used in this investigation consists of a Ag(111) crystal measuring 53 nm × 53 nm × 27 nm. Two different shapes of the local samples were used for a single impact depending on the symmetry of a developing cascade. The sample used to simulate 20-keV Au_3 impacts at normal incidence was cylindrical in shape with a radius of 8 nm and a height of 17 nm measured from the bottom of the deepest valley present in the local sample. All other impacts were calculated on samples that were a combination of a cylinder with a radius of 9 nm and a height of 10 nm measured from the bottom of the deepest valley, capped at the bottom with a hemisphere of the same radius. This hemispherical modification is done to reduce the total number of atoms being simulated, and thus reducing the computation time needed. The size of the samples was chosen based on visual observations of the size of collision cascades stimulated by impacts of 20-keV Au_3 and C_{60} projectiles on Ag(111) respectively. Rigid and stochastic regions measuring 0.7 and 2.0 nm, respectively, were used on the bottom as well as cylindrically around the sides to simulate the thermal bath that keeps the sample at required temperature, to prevent pressure waves, and to maintain the shape of the sample.[5,21] These outer layers also act as a sleeve that allows for the reinsertion of the modified coordinates back into the main sample without causing particles to overlap at the edges. 20-keV C_{60} and Au_3 projectiles were directed onto each sample at 0° and 70° with respect to the normal to the original surface. Atoms in the projectile had zero velocity relative to the center of mass of the cluster. A molecular dynamics/Monte Carlo-corrected effective medium (MD/MC-CEM) potential was used to describe the Ag−Ag interactions during C_{60} bombardment.[45] However, as this potential has known problems when describing interactions in metal alloys,[5] the embedded atom potential (EAM) was used to represent Ag−Ag, Ag−Au, and Au−Au interactions during Au_3 impacts.[46] The interaction between C atoms in the projectile were described by the adaptive intermolecular potential, AIREBO.[47] Finally, the interactions between C and Ag atoms were described by a weak Lennard-Jones potential[23] splined at small distances with a purely repulsive Moliere potential to better describe high energy collisions. A total of 800 impacts were performed per $(53\ nm)^2$ which corresponds to a fluence of $\sim 2.9 \times 10^{13}$ impacts/cm^2. Each individual impact was followed for 20 ps. This amount of time was sufficient to allow the roughly 10 ps collision process to occur and then allow the sample to equilibrate. Each 20 ps simulation required approximately two and six hours of CPU time on a 3.0 GHz Intel Xeon 3160 (Woodcrest) Dual-Core Processors for 20 keV Au_3 and C_{60}, respectively. We have used a flat surface and a surface previously modified by 800 consecutive impacts of clusters in order to calculate and compare kinetic energy and angular distributions of ejected species. These surfaces were irradiated at various points by 150 projectiles to increase statistical accuracy. Also in this case, individual impacts were simulated for 20 ps. Although this time is sufficient to contain sputtering phenomena taking place at the surface, it is much smaller than the time needed for sputtered particles to reach the detector in the experiment. Consequently, ejected clusters at the end of the simulation may have sufficient internal energy to unimolecularly decay.[48,49] To minimize the influence of this phenomenon on our spectra and to maintain a tractable computer time, we have divided the simulation into two time regimes. In the first time regime, the movements of all particles in the system were traced until 20 ps. In the subsequent regime, only the movements of sputtered particles were followed up to 500 ps. The calculations performed by Wucher and Garrison show that most of the ejected unstable silver clusters decompose into stable fragments on a time scale of several tens of picoseconds.[48,49] Therefore, we believe that the adopted time limit is sufficient to take into account the significant portion of these events. All kinetic energy and angular spectra presented in this paper were calculated from the corrected data.

Finally, there are disparate time scales between successive impacts in the simulations and experiment. The time between successive hits at overlapping impact areas in the simulation can be as short as tens of picoseconds whereas in the experiment the time is on the order of microseconds to milliseconds depending on the ion current. On this microsecond to millisecond time scale, thermal diffusion of material subsequent to the bombardment event is possible. The current MD simulations include all atomic motion to ~20 ps at which time the material is equilibrated and thus provides a starting point for possible thermal motion to occur. However, the thermal diffusion coefficient for Ag at ~560 K is 3×10^{-18} cm^2/s.[50] This small value indicates that diffusion would be at most a small contributor to interlayer mixing in this system at room temperature and is meaningless in experiments performed at liquid-nitrogen temperatures.

Results and Discussion

Morphology. Typical craters created by an impact of 20 keV Au_3 and C_{60} projectiles at a flat surface are shown in Figure 1 for normal and oblique impact angles. The presented craters were created during impacts that result in a sputtering yield close to the average value. It is evident that the size of the craters depends both on the type of the projectile and on the impact angle. The crater formed by an impact of a 20-keV Au_3 cluster at normal incidence is elongated in the vertical direction with a relatively small opening. Although, the crater extends deep into the sample a large fraction of the primary kinetic energy is deposited below the crater depth and cannot contribute to sputtering. While not contributing to ejection, this energy leads to a significant interlayer mixing.[23] The crater is surrounded by whiskers of melted and resolidified material that extend into the vacuum. These structures are particularly visible for 70° impact angle and indicate that during Au_3 impact a volume of very large density of primary energy is formed and that this energy is not redistributed isotropically. The crater formed by a normal impact of 20-keV C_{60} has a larger opening diameter and is shallower than the corresponding crater formed by 20-keV Au_3 impact. The crater is also more azimuthally isotropic and the overhanging features are not present. The increase of the impact angle results in a decrease of the crater depth for both Au_3 and C_{60}. However, this is where the similarity ends. While the lateral dimensions of the crater are significantly increased for Au_3 projectile bombarding Ag surface at 70°, the

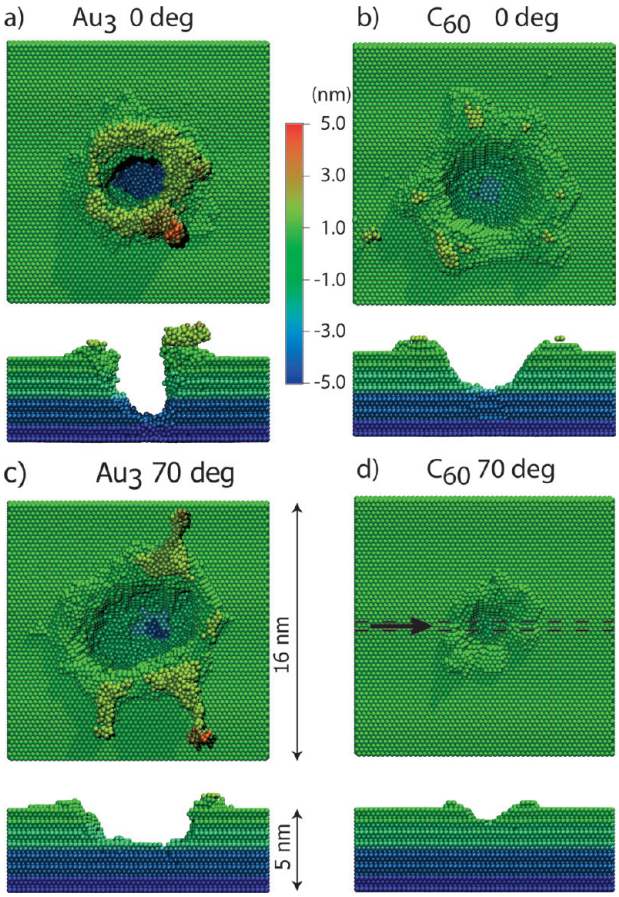

Figure 1. Top and cross sectional side views of typical craters created by impact of 20 keV: (a) Au_3 and (b) C_{60} at normal incidence and (c) Au_3 and (d) C_{60} at 70° impact angle at a flat Ag(111) surface at time of 20 ps. Colors scheme depicts final elevation of atoms spanning from −5 nm (blue) to +5 nm (red) relatively to the original surface plane. The cross sectional view is 1.5 nm wide (as indicated be dashed lines in panel d) and is centered along the projectile impact point. The arrow in panel d indicates azimuthal direction of the projectile impact for oblique incidence.

opposite trend is visible for C_{60}. The crater created by oblique Au_3 impact becomes ellipsoidal in shape with a longer axis almost parallel to the impact azimuth. Although, some lateral anisotropy is also present for 20-keV C_{60} at 70°, the eccentricity of the crater opening is small and the shape of the crater rim is rather insensitive to the impact angle. A similar behavior has been reported in C_{60} angle of incidence dependence study performed on organic systems.[51,52]

The difference of shapes of the craters formed by Au_3 and C_{60} projectiles is a consequence of a different initial history of the penetrating clusters. Due to its large size C_{60} projectile interacts strongly with the sample atoms. The process is almost mesoscopic in that the interaction of a C_{60} projectile with the rest of the system is a many body collision in which several projectile atoms simultaneously hit the same target atom.[19,31,53] The individual atoms in the cluster are not initiating their own collision cascades; rather they are working cooperatively to move the target atoms. One of the consequences of such activity is the generation of pressure waves that propagate in the sample.[19,21] After impact of the C_{60} projectile on the Ag surface, the spatial correlation of C atom movements is lost almost immediately. Due to the heavier mass of the Ag atoms, most of the C atoms originating from the projectile are reflected toward the vacuum. Consequently, the energy of the cluster projectile is deposited in a shallow volume of the sample in a short time, leading to the ejection of many particles. As a result, a large but relatively shallow and azimuthally isotropic crater is formed. The energy dependence studies show that the size of the crater, and consequently, the total sputtering yield decreases with a decrease of the initial kinetic energy.[23,26,54] The diameter of the crater is predominantly affected while its depth is much less reduced.[23]

A different scenario takes place during Au_3 bombardment. While the C_{60} shatters and the direction of motion of the individual carbon atoms quickly randomizes due to multiple collisions, the downward movement of gold atoms in most cases remain coordinated for a long time.[26,55] This difference in behavior is primarily due to two main factors: energy per projectile particle and projectile atom mass versus substrate atom mass. Each carbon atom composing the 20-keV C_{60} cluster, has 333 eV of kinetic energy and a mass of 12 amu, and is traveling with a momentum 18 times smaller than that of a gold atom from 20-keV Au_3 projectile, which has a kinetic energy of 6667 eV and a mass of 197 amu. Thus, the carbon atoms are more easily deflected by the 107 amu Ag atoms. As a consequence, at the end of the first picosecond, all of the downward momentum of the fullerene molecule is appreciably reduced and each carbon atom is confined to the evacuated crater region of 3 nm deep or less. Conversely, the gold atoms are heavier than the silver atoms. Some of them, therefore, travel deep into the sample depositing their kinetic energy over a significant depth. For instance, for the trajectory shown in Figure 1a, the crater extends up to 3.5 nm while the three Au atoms are implanted at a depth of 2.3, 6.7, and 16.3 nm, respectively. One consequence of such behavior has already been mentioned; that is, an elongated shape of the crater and a lower sputtering yield as compared to corresponding C_{60} impact. Another consequence is a much larger effect of the increasing impact angle observed for the Au_3 projectile as compared to the C_{60} cluster. The average penetration depth of the 20-keV Au_3 projectile is significantly altered when the impact angle changes from 0° to 70°. As a result, the energy deposition profile shifts closer to the surface and a larger portion of the primary kinetic energy can be deposited in the volume that actually can contribute to sputtering.[51,56,57] For a wide range of impact angles, the energy reflection process has only a modest role on the sputtering yield for heavy Au atoms. As a result, the total sputtering yield increases when the impact angle is increased. Only at large impact angles does the energy reflection begin to dominate and the efficiency of erosion decreases.[57] We have found that the calculated sputtering yield is almost constant up to 30°. At larger angles it begins to rise significantly, reaching a pronounced maximum around 65°. Contrary to Au_3 bombardment, the primary kinetic energy is already deposited in a shallow volume for the fullerene projectile at normal incidence. Therefore, an increase of the impact angle will not supply any additional energy in the active region. On the other hand, the effect of an increased reflection of the primary kinetic energy is more severe for light projectile atoms. As a result, the total sputtering yield of Ag due to C_{60} bombardment has a wide and flat maximum around 30° and the signal begins to decrease at larger impact angles.[23]

If the general trends observed during individual impacts on a flat surface were preserved during continuous irradiation, one would expect to see a significant difference in the topography of the irradiated surface. The resulting surface topography obtained after 800 impacts (fluence 2.9×10^{13} impacts/cm^2) of 20-keV Au_3 and C_{60} at 0° and 70° impact angles are shown in Figure 2. Indeed, there are significant differences between

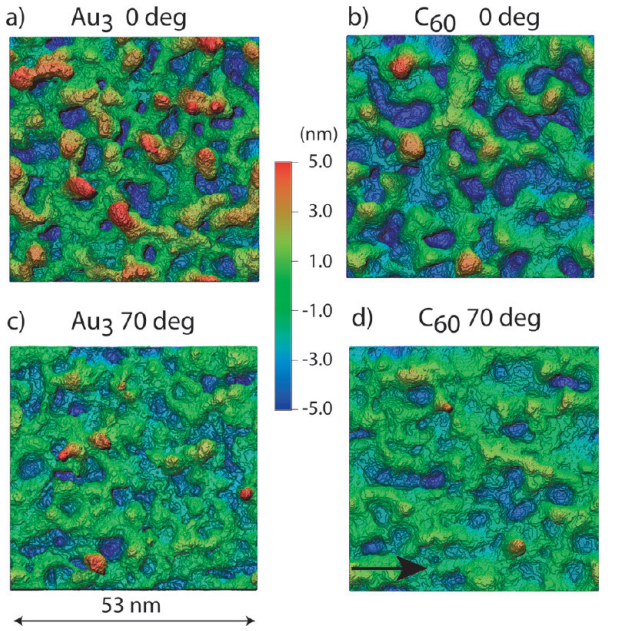

Figure 2. Top view at the surface topography created after 800 impacts (fluence of ~2.9 × 10^{13} impacts/cm^2) of 20 keV: (a) Au_3 and (b) C_{60} at normal incidence and (c) Au_3 and (d) C_{60} at 70° impact angle. Colors scheme depicts final elevation of atoms spanning from −5 nm (blue) to 5 nm (red) relatively to the original surface plane. The arrow in panel 2d indicates azimuthal direction of the projectile impact for oblique incidence.

surfaces sputtered by Au_3 and C_{60} projectiles. There is also a quite pronounced effect of the impact direction. As expected from the data shown in Figure 1, the most corrugated surfaces are formed after irradiation with Au_3 clusters at normal incidence. The created structures are narrower than analogous structures formed after C_{60} bombardment and have a larger difference between the lowest and the highest elevations (~20 nm for Au_3 and ~14 nm for C_{60} at normal impact angle). The oblique irradiation leads, in general, to a less corrugated surface as compared to the normal bombardment. The least corrugated surface is achieved during 20-keV C_{60} irradiation at 70° impact angle. However, even in this case, surface modification is still significant. After the impact of 800 clusters, there are only small parts of the crystals that remain flat. The surface is composed of a network of monoatomically high atomic terraces that form valleys and mound-like structures. A closer inspection of the data presented in Figure 2 shows that silver atoms retain their original arrangement in these areas. The spatial orientation of the surface valleys is correlated with the azimuthal direction of clusters impinging at 70°.

At the fluence of 2.9 × 10^{13} impacts/cm^2, the average level of the bombarded surface has shifted by 1.95 and 1.06 nm downward for 20-keV C_{60} at 0° and 70° incidence and 1.34 and 1.29 nm for 20-keV Au_3 at 0° and 70° incidence, respectively. At low fluencies, however, we observe that the average surface level is actually increased. Such surface swelling was observed experimentally and is attributed to projectile atom implantation and/or amorphization/randomization of the irradiated structure.[58−61] The second process is more probable in our case particularly for C_{60} where atom implantation is low[23] and carbon atoms are also smaller than Ag atoms. It is also very interesting to note that, apart from the average surface retraction observed at 2.9 × 10^{13} impacts/cm^2, there are many areas that actually extend way above the original surface level. The effect is particularly strong for Au_3 at normal incidence where many narrow, stalagmite-like structures rise up to 5 nm above the original surface level. The structures created by 20-keV C_{60} impact at normal incidence are wider and lower than the ones obtained during Au_3 irradiation. Nevertheless, some of these structures also protrude into the vacuum above the original surface level.

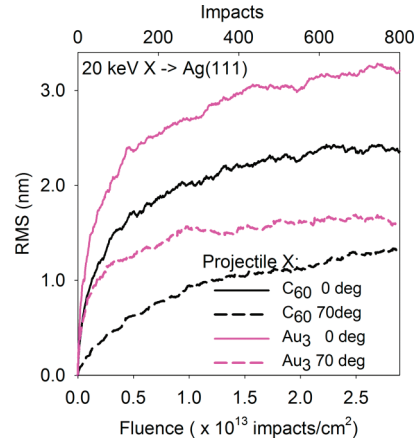

Figure 3. Root-mean-square roughness in nanometers of the entire sample versus the number of projectile impacts and the ion beam fluence. Dash-dotted, solid, dashed, and dotted lines represent 20 keV Au_3, C_{60} at normal incidence and Au_3 and C_{60} at 70° impact angle, respectively.

To compare more quantitatively the evolution of the irradiated surface, the root-mean-square (rms) roughness of the investigated systems is calculated. The variation of the rms as a function of the number of impacts or a fluence is shown in Figure 3. To calculate the rms roughness, the sample was discretized into 0.42 nm by 0.42 nm columns, with each column giving a surface height value. This size was chosen in order to be as small as possible for accuracy but large enough so as not to obtain measurements of zero between crystal lattice rows. Two trends can be identified in the development of surface roughness. First, at the beginning, the value of the rms increases fast. This fast increase is followed by a slow increase that finally goes into saturation. We attribute the initial fast increase to the fact that the roughness of the sample is rapidly changing due to the (artificially) flat surface starting conditions. This phase then moves into the more natural, slow decay caused by multiple bombardments. With this trendline, the estimated final roughness value is 2.5 and 1.3 nm for 20-keV C_{60} at 0° and 70°, and 3.2 and 1.6 nm for 20-keV Au_3 projectile at 0° and 70° impact angles, respectively. Not surprisingly, the largest rms is achieved by 20-keV Au_3 projectiles at normal incidence. The modification of the impact angle has a larger influence on the rms evolution for 20-keV C_{60} than for Au_3 projectiles.

While the rms can give some valuable hints about the evolution of irradiated surface, its applicability is limited because it gives information about the whole surface and is not sensitive to a local topography. One of very important factors for many ion-beam applications is the height distribution and/or the lateral size distribution of the created structures as they will be sputtered in different ways. In our previous publication, we have investigated how sputtering of various structures influences the local roughness conditions.[39] Several various possibilities were identified. The defining topographical feature that produces an increase in the roughness is an impact that occurs within a depression or preexisting crater. In this case, the crater is becoming deeper and the majority of the ejected material is redeposited at the surrounding walls. Conversely, an impact at the convex structures produces a decrease in roughness. In this case, there are two processes that will reduce local roughness.

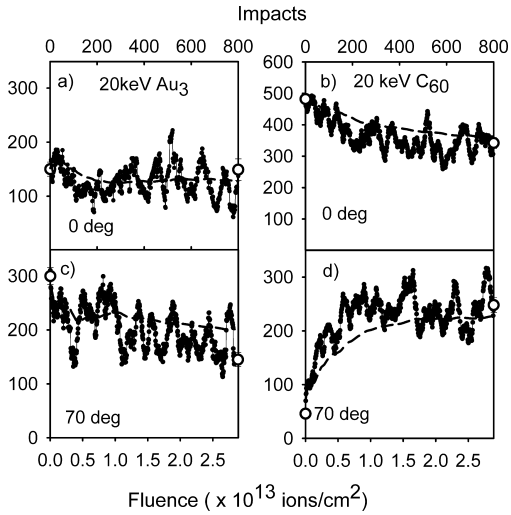

Figure 4. Dependence of the total sputtering yield on the number of impacts and the ion beam fluence for 20 keV: (a) Au_3 and (b) C_{60} at normal incidence and (c) Au_3 and (d) C_{60} at 70° impact angle at Ag(111). Dashed line represents the total sputtering yield calculated as an accumulated mass removal per single projectile. Open circles represent the total sputtering yields calculated from 150 impacts at a flat surface and a surface preirradiated with 800 projectiles.

First, the elevation or mound is usually destroyed. Because there is no bulk material surrounding it, the mound particles are ejected outward from the impact in all directions where the vacuum is present. Some of this material is sputtered; however, the majority of the particles contact the surface and the adjacent crater wall, effectively filling in the crater. Within this interpretation, the final effect will depend on the relative contribution of hills and valleys. It would be important, therefore, to have some metrology that could not only estimate the global vertical corrugation of altered surfaces but also give some information about local dimensions of the created structures. For instance, the set of data that was used to calculate the rms could be used to draw a histogram of the discretized surface elevations or the histogram of the lateral size of created structures. Making such analysis lies, however, outside the main scope of this paper and will be discussed more thoroughly in another publication.

Sputtering Yield. Dependence of the sputtering yields on the projectile fluence for 20-keV Au_3 and C_{60} at 0° and 70° is shown in Figure 4. Each point in the figure represents the averaged value of 30 consecutive impacts (a running average) to reduce statistical uncertainty. The dashed line represents the total sputtering yield calculated from the accumulated material removal. This quantity is usually measured in experiments with a graphite collector, a microbalance, or STM/AFM probes.[57] The open circles indicate the sputtering yields calculated as an average of 150 impacts at a flat surface and at a preirradiated surface. It is evident that the evolution of the sputtering yield depends on the projectile type and the impact angle. For 20-keV Au_3 irradiation at 0° and 70° impact angles and for 20-keV C_{60} impacts at normal incidence, the total sputtering yield obtained from the accumulated material removal, indicated by a dashed line in Figure 4, decreases with the fluence in the low fluence regime. A comparison with the data shown in Figures 3 and 4 indicates that there is a similarity in the rate of rms change and the rate of decrease of the sputtering yield calculated from accumulated mass deficit. In both cases, a fast and slow component can be identified, with the transition point from fast to slow occurring roughly at the same fluence ($\sim 5 \times 10^{12}$ /cm^2). It is justifiable, therefore, to conclude that the yield depends on the surface topography. While the average values of the total sputtering yield changes monotonically, there is a significant variation of the instantaneous values of this quantity which has a form of almost periodic oscillations. Although, there is a correlation between the increase of the rms and a decrease of the total sputtering yield calculated by a mass deficit, there is no evident relation between the rms curve and the total yield oscillations. However, as was previously discussed, the rms represents global modifications, while the instantaneous value of the total sputtering yield will be sensitive mostly to the local environment. At this time, we are not certain what the reason is of such large yield oscillations.

TABLE 1: Total Sputtering Yields Calculated at Ag(111) Bombarded with 20 keV Au_3 and C_{60} at 0° and 70° Impact Angles, and with 6.67 keV Au Projectiles at Normal Incidence[a]

projectile	Y (flat surface)	Y (preirradiated surface)
20 keV C_{60}	482 ± 8	342 ± 17
20 keV C_{60} 70°	46 ± 1.4	258 ± 14
20 keV Au_3	143 ± 13 (141)	142 ± 20
20 keV Au_3 70°	300 ± 16	145 ± 13
6.67 keV Au	16 ± 2	15 ± 1

[a] The values are an average of 150 impacts at a flat Ag(111) surface and a surface that was preirradiated by consecutive 800 impacts, which corresponds to a fluence of 2.3×10^{13} impacts/cm^2.

It is also interesting to note that the total sputtering yield calculated on a flat surface for 20-keV Au_3 projectiles at 70° is larger than for normal impact which is opposite to the trend calculated for C_{60}. The calculation performed at a flat surface for 20-keV Au_3 impacts shows that the maximum of the sputtering yield occurs around 65° impact angle. Such a behavior was observed in many experiments with atomic projectiles. It is a consequence of the fact that the deposited energy profile is elongated and a substantial fraction of the primary kinetic energy is deposited too deep to contribute to sputtering.[57,62] Because most of the primary kinetic energy is already deposited in an active volume that contributes to sputtering for C_{60} at normal incidence, an increase of the impact angle will result only in a modest signal enhancement. The signal enhancement will soon be reduced due to a decrease of the density of the deposited energy caused by an efficient reflection of C atoms arriving at the surface at larger impact angles. The average amount of reflected kinetic energy changes from 2.6-keV (20-keV C_{60}) and almost 0-keV (20-keV Au_3) at normal incidence to 13.7-keV (20-keV C_{60}) and 3.2-keV (20-keV Au_3) for 70° impact angle. The impact-angle dependence of the total sputtering yield indicates that the Au_3 clusters behave more like atomic projectiles, regardless of the fact that the nonlinear enhancement of the total sputtering yield is present as shown in Table 1. The accumulated effect of three separate impacts of 6.67-keV Au atoms composing a 20-keV Au_3 cluster results in 45 sputtered Ag atoms. The total sputtering yield of a single 20-keV Au_3 impact is ~143, which is three times larger. The effect is smaller than for 20-keV C_{60} impact at normal incidence where a 5-fold yield enhancement was reported.[23] Recently it has been reported that the sputtering yield induced by collimated Ar^+ beam irradiating stepped surface at oblique incidence can increase significantly due to planar channeling.[63,64] However, we do not expect that a similar process can be efficient in our case due to a larger size of the impinging projectiles.

A quite different variation of the sputtering yield with the fluence occurs for C_{60} projectiles bombarding the surface at 70° impact angle. As shown in Figure 4d, the sputtering yield strongly increases with the fluence. As shown in Table 1, the

yield calculated on a flat surface is almost six times smaller than the average yield obtained at a preirradiated sample. Also in this case, the comparison of the data presented in Figures 3 and 4d shows that the modification of the total sputtering yield occurs in the fluence region of the fastest rms variation, but now there is a direct correspondence. Such different behavior is once again a consequence of a specific energy deposition profile of the C_{60} cluster. Due to a mass difference between carbon and silver atoms and a very large impact angle most of the primary kinetic energy is reflected into the vacuum when bombarding the flat surface. In fact, more than 15 keV of the primary kinetic energy is reflected under these conditions. As a result, for 20-keV C_{60} at 70°, only a small fraction of the primary kinetic energy can be used to stimulate ejection and the sputtering yield is small. As the surface is getting rougher, the local impact angle is reduced. As a consequence, the reflection process is reduced, more primary kinetic energy can be deposited in the subsurface volume, and the sputtering yield increases. We see that only around 6.7 keV of the primary energy is reflected from preirradiated surface. It should be pointed out, however, that the variation of an average local impact angle is only one parameter that influences sputtering efficiency. As was already discussed, development of the complicated surface morphology composed of hills and valleys also plays a profound role. For instance, clusters impinging at a large off-normal angle can shear protruded structures leading to ejection of large chunks of material.

The results presented in Figure 4 allow us to draw the following predictions. The experimentally determined total sputtering yields, which usually involves measurements on a system irradiated with more than 10^{13} impacts/cm^2, will not depend on the fluence. However, the yields calculated on flat surfaces are rather poor estimates of the yields measured in experiments done in dynamic conditions. The calculations performed on flat surfaces at normal incidence will overestimate the experimental values. The amount of this overestimation will increase with the projectile size at normal incidence. A particularly large error can be made if one attempts to extend the results of flat surface yield calculations to the experimental results obtained for oblique incidence of medium or large clusters.

Kinetic Energy Distributions. The kinetic energy distributions of sputtered Ag atoms and Ag_2 dimers calculated for 20-keV Au_3 and C_{60} projectiles at 0° are shown in Figure 5. The results for 70° impact exhibit similar trends as the kinetic energy spectra obtained for normal impact. Therefore, they are not shown here. It is evident from Figure 5 that the shape of the kinetic energy spectra is insensitive to the variation of surface topography. In general, the Ag atoms are ejected with higher kinetic energies during Au_3 irradiation than for C_{60}. The most interesting difference however, is the behavior of Ag and Ag_2 spectra stimulated by irradiation of Au_3 and C_{60} projectiles. The maximum in the kinetic energy distribution of Ag_2 is shifted to lower kinetic energy for 20-keV Au_3, whereas the opposite trend is observed for 20-keV C_{60}. The shift observed for fullerene clusters has already been reported both in simulations[7] and in experiment.[22,23,65] It is attributed to the mesoscopic character of ejection processes which cause that the sputtering mechanism resembles a hydrodynamic gas flow of excited material.[66,67] In such process, all particles are ejected with similar velocities which results in a larger kinetic energy of the heavier components. In contrary to the behavior observed during C_{60} irradiation, the kinetic energy distributions of Ag_2 ejected by 20-keV Au_3 impacts are shifted to lower kinetic energy as compared to

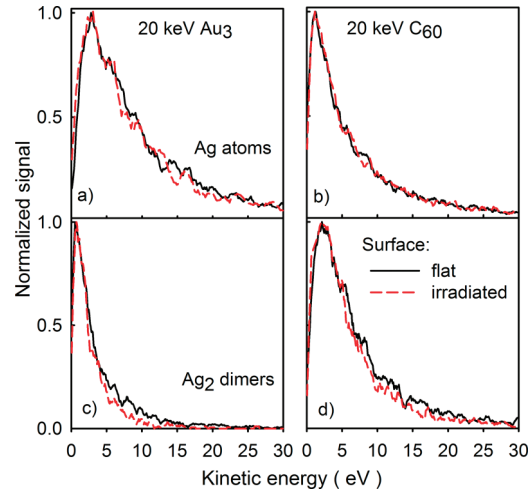

Figure 5. Kinetic energy distributions of Ag atoms sputtered with 20 keV (a) Au_3 and (b) C_{60}, and Ag_2 dimers sputtered with 20 keV (c) Au_3 and (d) C_{60} at 0° impact angle at a flat (solid line) Ag(111) surface, and a surface preirradiated with 800 projectiles (dashed line).

the spectra of Ag. Such behavior is typically observed during atomic bombardment, where the density of deposited energy is not large enough to create excited volume with a sufficient density to stimulate gas flow. In this case, the main role is played by a decay of internally excited dimers which leads to a depletion of the kinetic energy spectrum of the high energy molecules, shifting it to lower kinetic energies.[23,48,49,68,69] It seems that while a nonlinear enhancement is visible for Au_3, a strong binding energy of Ag may prevent the creation of a volume with energy density high enough to stimulate hydrodynamic ejection. This supposition could explain why Samartsev and Wucher[65] have actually observed similar velocity distributions of In and In_2 dimers ejected from polycrystalline In foil bombarded with 10-keV Au and Au_2 projectiles. The material binding energy is much lower for In which means that a larger number of atoms will be set in motion.

Nevertheless, apart from this interesting difference, the main conclusion that can be drawn from the data shown in this paragraph is that the shape of the kinetic energy distributions does not depend on the surface topography. As a result, the kinetic energy spectra calculated on a flat surface can be directly compared to the experimental spectra obtained even under dynamic conditions.

Angular Distributions. The polar angle distributions of Ag atoms sputtered by 20-keV Au_3 and C_{60} projectiles at 0° and 70° are shown in Figure 6. Contrary to the kinetic energy distributions, angular spectra are strongly influenced by the development of surface topography. It is interesting to note that the angular distribution of Ag atoms sputtered by 20-keV Au_3 from a flat surface shows azimuthal and polar anisotropy that is again characteristic to sputtering of single crystals by atomic projectiles.[70] The anisotropy disappears, however, after extensive bombardment as the irradiated surface resembles more a surface of a polycrystalline target than a surface of a single crystal (see Figure 2).

The polar angle distributions of Ag atoms sputtered from a flat surface by 20-keV C_{60} at normal incidence do not show a structure characteristic for a single crystal sputtering. This is a consequence of the previously discussed mesoscopic character of the ejection process induced by medium size clusters. As shown by numerous studies, arrangement of atoms in the irradiated volume of the single crystal is destroyed almost immediately after the cluster impact and the particles are ejected

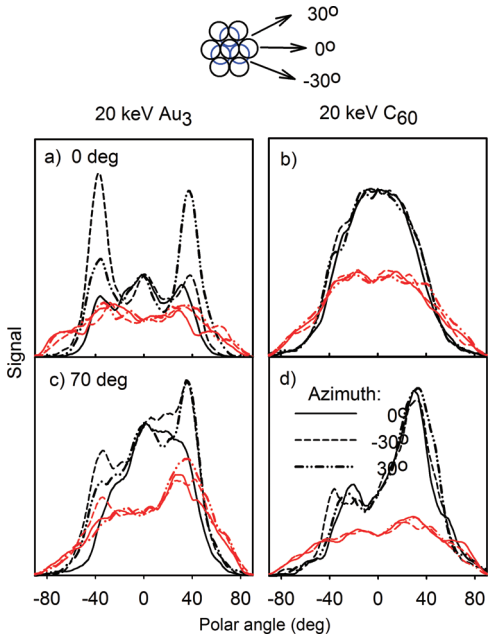

Figure 6. Polar angle distributions of Ag atoms sputtered with 20 keV (a) Au_3 and (b) C_{60} at normal incidence and (c) Au_3 and (d) C_{60} at 70° impact angles. The data are shown for three different azimuths as indicated at the top of the figure. Black and blue circles depict first and second layer atoms, respectively. Black lines represent results of calculations performed on a flat surface, while red curves represent results of studies done at a surface preirradiated with 800 projectiles.

from a randomized volume.[19,23,26,71] As a result, the ejection is azimuthally isotropic and concentrated along the normal to the surface as seen in Figure 6b. Modification of the surface structure by extensive irradiation results in more versatile ejection possibilities and, consequently, in a less concentrated emission. The ejection occurs at larger angles for both Au_3 and C_{60}. The angular distributions of particles ejected from flat surfaces by an oblique impact of both C_{60} and Au_3 projectiles exhibits a memory of the initial impact direction. Most of the particles are sputtered toward the direction that is almost specular to the original impact angle. In this case, an extended irradiation leads to a significant reduction of this memory effect and the angular spectra resemble more distributions obtained during sputtering of preirradiated surface at 0° impact angle.

Conclusions

We have examined the effect of the continuous irradiation by 20-keV Au_3 and C_{60} projectiles on the development of surface topography, and the sputtering ejection characteristics usually measured in experiments. There are several predictions that result from our studies. First, the Au_3 cluster behaves in some aspects like an atomic projectile when bombarding the Ag sample. This indicates that both the experimental and theoretical results obtained with these clusters should be used with caution when discussing properties of the sputtering processes initiated by medium and large size clusters. Second, both the sputtering yield and the angular spectra are sensitive to the ion fluence. Therefore, it is not justifiable to project results of calculations of these quantities obtained at flat surfaces to the experiments performed in dynamic conditions. Finally, the kinetic energy distributions are not sensitive to the development of the surface topography. Therefore, the kinetic energy distributions calculated at a flat surface are a good representation of the results obtained in experiments performed even in dynamic conditions.

Acknowledgment. The authors thank the Polish Ministry of Science and Higher Education programs No. PB 4097/H03/2007/33 and PB 0935/B/H03/2008/35 and the Chemistry Division of the National Science Foundation Grant No. CHE-0910564 for their financial support of this research. The authors also thank The Pennsylvania State University High Performance Computing Group for use of their computing resources and technical support. The visualization of the data presented in Figures 1 and 2 was done with free VMD[72] and MSMS[73] software.

References and Notes

(1) Thompson, D. A.; Johar, S. S. *Appl. Phys. Lett.* **1979**, *34*, 342.
(2) Thompson, D. A.; Johar, S. S. *Radiat. Eff. Defects Solids* **1981**, *55*, 91.
(3) Andersen, H. H. *Vidensk. Selsk. Mat. Fy.* **1993**, *43*, 127.
(4) Urbassek, H. M. Results of molecular dynamics calculations. In *Sputtering by Particle Bombardment*; Springer: Berlin, 2007; Vol. 110, p 189.
(5) Garrison, B. J.; Postawa, Z. *Mass Spectrom. Rev.* **2008**, *27*, 289.
(6) Gillen, G.; Fahey, A.; Wagner, M.; Mahoney, C. *Appl. Surf. Sci.* **2006**, *252*, 6537.
(7) Wucher, A.; Cheng, J.; Winograd, N. *Anal. Chem.* **2007**, *79*, 5529.
(8) Shard, A. G.; Green, F. M.; Brewer, P. J.; Seah, M. P.; Gilmore, I. S. *J. Phys. Chem. B* **2008**, *112*, 2596.
(9) Jones, E. A.; Lockyer, N. P.; Vickerman, J. C. *Anal. Chem.* **2008**, *80*, 2125.
(10) Wucher, A.; Cheng, J.; Zheng, L.; Winograd, N. *Anal. Bioanal. Chem.* **2009**, *393*, 1835.
(11) Fuoco, E. R.; Gillen, G.; Wijesundara, M. B. J.; Wallace, W. E.; Hanley, L. *J. Phys. Chem. B* **2001**, *105*, 3950.
(12) Weibel, D.; Wong, S.; Lockyer, N.; Blenkinsopp, P.; Hill, R.; Vickerman, J. C. *Anal. Chem.* **2003**, *75*, 1754.
(13) Gillen, G.; King, L.; Freibaum, B.; Lareau, R.; Bennett, J.; Chmara, F. *J. Vac. Sci. Technol. A* **2001**, *19*, 568.
(14) Winograd, N. *Anal. Chem.* **2005**, *77*, 142A.
(15) Wucher, A. *Appl. Surf. Sci.* **2006**, *252*, 6482.
(16) Vickerman, J. C. *Surf. Sci.* **2009**, *603*, 1926.
(17) Smith, R.; Webb, R. P. *Proc. R. Soc. London Ser. A* **1993**, *441*, 495.
(18) Smith, R.; Beardmore, K. *Thin Solid Films* **1996**, *272*, 255.
(19) Seki, T.; Aoki, T.; Tanomura, M.; Matsuo, J.; Yamada, I. *Mater. Chem. Phys.* **1998**, *54*, 143.
(20) Webb, R.; Kerford, M.; Way, A.; Wilson, I. *Nucl. Instrum. Methods Phys. Res., Sect. B* **1999**, *153*, 284.
(21) Postawa, Z.; Czerwinski, B.; Szewczyk, M.; Smiley, E. J.; Winograd, N.; Garrison, B. J. *Anal. Chem.* **2003**, *75*, 4402.
(22) Sun, S.; Szakal, C.; Smiley, E. J.; Postawa, Z.; Wucher, A.; Garrison, B. J.; Winograd, N. *Appl. Surf. Sci.* **2004**, *231*−*2*, 64.
(23) Postawa, Z.; Czerwinski, B.; Szewczyk, M.; Smiley, E. J.; Winograd, N.; Garrison, B. J. *J. Phys. Chem. B* **2004**, *108*, 7831.
(24) Delcorte, A. *Phys. Chem. Chem. Phys.* **2005**, *7*, 3395.
(25) Zimmermann, S.; Urbassek, H. M. *Nucl. Instrum. Methods B* **2005**, *228*, 75.
(26) Anders, C.; Urbassek, H. M. *Nucl. Instrum. Methods Phys. Res., Sect. B* **2005**, *228*, 57.
(27) Krantzman, K. D.; Kingsbury, D. B.; Garrison, B. J. *Appl. Surf. Sci.* **2006**, *252*, 6463.
(28) Webb, R.; Chatzipanagiotou, A. *Nucl. Instrum. Methods Phys. Res., Sect. B* **2006**, *242*, 413.
(29) Szakal, C.; Kozole, J.; Russo Jr, M. F.; Garrison, B. J.; Winograd, N. *Phys. Rev. Lett.* **2006**, *96*, 216104.
(30) Delcorte, A.; Garrison, B. J. *J. Phys. Chem.* **2007**, *111*, 15312.
(31) Zimmermann, S.; Urbassek, H. M. *Nucl. Instrum. Methods Phys. Res., Sect. B* **2007**, *255*, 208.
(32) Anders, C.; Kirihata, H.; Yamaguchi, Y.; Urbassek, H. M. *Nucl. Instrum. Methods Phys. Res., Sect. B* **2007**, *255*, 247.
(33) Samela, J.; Nordlund, K. Physical Review B 2007, *76*.
(34) Henriksson, K. O. E.; Nordlund, K.; Keinonen, J. *Nucl. Instrum. Methods Phys. Res., Sect. B* **2007**, *255*, 259.
(35) Russo, M. F.; Ryan, K. E.; Czerwinski, B.; Smiley, E. J.; Postawa, Z.; Garrison, B. J. *Appl. Surf. Sci.* **2008**, *255*, 897.
(36) Samela, J.; Nordlund, K. Phys. Rev. Lett. 2008, *101*.
(37) Krantzman, K. D.; Webbb, R. P.; Garrison, B. J. *Appl. Surf. Sci.* **2008**, *255*, 837.
(38) Krantzman, K. D.; Garrison, B. J. *Nucl. Instrum. Methods Phys. Res., Sect. B* **2009**, *267*, 652.
(39) Russo, M. F.; Postawa, Z.; Garrison, B. J. *J. Phys. Chem. C* **2009**, *113*, 3270.

(40) Hofer, W. O. *Top. Appl. Phys.* **1991**, *64*, 15.
(41) Hauffe, W. *Top. Appl. Phys.* **1991**, *64*, 305.
(42) Moseler, M.; Rattunde, O.; Nordiek, J.; Haberland, H. *Nucl. Instrum. Methods Phys. Res., Sect. B* **2000**, *164*, 522.
(43) Aoki, T.; Matsuo, J. *Nucl. Instrum. Methods Phys. Res., Sect. B* **2007**, *255*, 265.
(44) Aoki, T.; Matsuo, J.; Yamada, I. *I. Mater. Res. Soc. Symp. Proc.* **2004**, 792.
(45) Kelchner, C. L.; Halstead, D. M.; Perkins, L. S.; Wallace, N. M.; Depristo, A. E. *Surf. Sci.* **1994**, *310*, 425.
(46) Foiles, S. M.; Baskes, M. I.; Daw, M. S. *Phys. Rev. B* **1986**, *33*, 7983.
(47) Stuart, S. J.; Tutein, A. B.; Harrison, J. A. *J. Chem. Phys.* **2000**, *112*, 6472.
(48) Wucher, A.; Garrison, B. J. *Phys. Rev. B* **1992**, *46*, 4855.
(49) Wucher, A.; Garrison, B. J. *J. Chem. Phys.* **1996**, *105*, 5999.
(50) Lam, N. Q.; Rothman, S. J.; Mehrer, H.; Nowicki, L. J. *Phys. Status Solidi B* **2006**, *57*, 255.
(51) Ryan, K. E.; Smiley, E. J.; Winograd, N.; Garrison, B. J. *Appl. Surf. Sci.* **2008**, *255*, 844.
(52) Ryan, K. E.; Garrison, B. J. *Anal. Chem.* **2008**, *80*, 5302.
(53) Czerwinski, B.; Samson, R.; Garrison, B. J.; Winograd, N.; Postawa, Z. *Vacuum* **2006**, *81*, 167.
(54) Anders, C.; Urbassek, H. M. *Nucl. Instrum. Methods Phys. Res., Sect. B* **2005**, *228*, 84.
(55) Russo, M. F., Jr.; Wojciechowski, I. A.; Garrison, B. J. *Appl. Surf. Sci.* **2006**, *252*, 6423.
(56) Ryan, K. E.; Garrison, B. J. *Anal. Chem.* **2008**, *80*, 5302.
(57) Eckstein, W. Sputtering yields. In *Sputtering by Particle Bombardment*; Springer-Verlag: Berlin, 2007; Vol. 110, p 33.
(58) Gnaser, H.; Brodyanski, A.; Reuscher, B. *Surf. Interface Anal.* **2008**, *40*, 1415.
(59) Lehrer, C.; Frey, L.; Petersen, S.; Ryssel, H. *J. Vac. Sci. Technol. B* **2001**, *19*, 2533.
(60) Yanagisawa, J.; Takarabe, K.; Ogushi, K.; Gamo, K.; Akasaka, Y. *J. Phys.-Condensed Matter* **2007**, *19*.
(61) Mutzke, A.; Eckstein, W. *Nucl. Instrum. Methods Phys. Res., Sect. B* **2008**, *266*, 872.
(62) Russo, M. F., Jr.; Szakal, C.; Kozole, J.; Winograd, N.; Garrison, B. J. *Anal. Chem.* **2007**, *79*, 4493.
(63) Hansen, H.; Redinger, A.; Messlinger, S.; Stoian, G.; Rosandi, Y.; Urbassek, H. M.; Linke, U.; Michely, T. *Phys. Rev. B* **2006**, *73*.
(64) Redinger, A.; Rosandi, Y.; Urbassek, H. M.; Michely, T. *Phys. Rev. B* **2008**, *77*.
(65) Samartsev, A. V.; Wucher, A. *Appl. Surf. Sci.* **2006**, *252*, 6470.
(66) Urbassek, H. M.; Michl, J. *Nucl. Instrum. Methods Phys. Res., Sect. B* **1987**, *22*, 480.
(67) Jakas, M. M.; Bringa, E. M.; Johnson, R. E. *Phys. Rev. B* **2002**, *65*, 165425.
(68) Chatterjee, R.; Postawa, Z.; Winograd, N.; Garrison, B. J. *J. Phys. Chem. B* **1999**, *103*, 151.
(69) Delcorte, A.; Bertrand, P.; Garrison, B. J. *J. Phys. Chem. B* **2001**, *105*, 9474.
(70) Wehner, G. K. *Phys. Rev.* **1956**, *102*, 690.
(71) Aderjan, R.; Urbassek, H. M. *Nucl. Instrum. Methods Phys. Res., Sect. B* **2000**, *164*, 697.
(72) Humphrey, W.; Dalke, A.; Schulten, K. *J. Mol. Graph.* **1996**, *14*, 33.
(73) Sanner, M. F.; Spehner, J. C.; Olson, A. J. *Biopolymers* **1996**, *38*, 305.

JP906139D